Microelectronics Reliability 53 (2013) 1002–1008

Contents lists available at SciVerse ScienceDirect

Microelectronics Reliability

journal homepage: www.elsevier.com/locate/microrel

# Role of impact ultrasound on bond strength and Al pad splash in Cu wire bonding

A. Rezvani [a,*], A. Shah [b], M. Mayer [a], Y. Zhou [a], J.T. Moon [c]

[a] Microjoining laboratory, University of Waterloo, Waterloo, ON, Canada
[b] Kulicke and Soffa Industries, Inc., Fort Washington, PA 19034, USA
[c] MK Electron Co. Ltd., Yongin, Republic of Korea

ARTICLE INFO

*Article history:*
Received 8 June 2012
Received in revised form 22 February 2013
Accepted 8 March 2013
Available online 3 May 2013

ABSTRACT

Cu wire is replacing Au wire in the microelectronic industry due to its lower cost. However, during Cu ball bonding one of the main challenges is the increased stress that can damage the pad and underpad layers. Past work showed that using ultrasound super-imposed together with impact force (pre-ultrasound) results not only in a softer bonded ball, but also in a flatter ball/pad interface. In this study, Cu ball bonding processes are optimized with five levels of pre-ultrasound. The wire material is 99.99% pure Cu wire, 25.4 μm in diameter. It is shown that by using pre-ultrasound of 37.5% bonds with adequately high shear strength (120 MPa) are achieved and the amount of splash is reduced by 31%. Using pre-ultrasound allows for lower bonding ultrasound levels that result in less stress on the pad and underpad materials.


## 1. Introduction

Thermosonic Au ball bonding is the main method for making interconnections between the semi-conductor chip and the package in microelectronics packaging [1–3]. In this process, a thin metal wire loop is welded to a metallic bond pad, by a combination of heat, normal pressure and ultrasonic energy. With the increasing trend of the price of Au, less expensive materials such as Cu are being considered for wire bonding as an alternative to the Au wire [4]. In addition to the lower cost, Cu possesses better electrical, thermal and mechanical properties than Au. However, using Cu wire has disadvantages [5–8]. Among them are the increased tendency to oxidize, narrow process window for second bond, and increased bonding stress transferred to underpad materials [1,9,10]. Because of the higher hardness of Cu wire, higher levels of bonding force and ultrasound are normally required to make good quality bonds compared to processes with Au wire which is softer. The higher levels cause an increase in the underpad stresses, which might consequently lead to pad/chip damage. The damage can occur as pad peeling [11,12], silicon cratering [13–15], and pad metal splash [16–18]. Pad metal splash is the pad metal extruded from the edges of the bonded ball. It is accompanied by pad thinning, and occurs mostly in the ultrasonic direction. The amount of splash increases with higher bond force and ultrasonic power. It is not a failure by itself but can reduce bond reliability because of pad material thinning. Pad metal splash is of particular concern in today's ultra fine pitch applications where it may cause shorting between the adjacent bonded balls pads [1,18,19].

Ball bonding can be described as a mixture of two processes types: Ultrasound Enhanced Deformation (UED) process and impact deformation process [9]. It has been shown that using superimposed ultrasound during the impact segment of an impact deformation process, also called pre-ultrasound, improves the deformability of free air ball, resulting in a softer bonded balls [20]. Softening occurs both during the ultrasound period (temporary acoustic softening) and also afterwards (residual softening). It is shown that the amount of this softening is proportional to the ultrasound amplitude. In [21], the authors investigated the effect of pre-ultrasound in Cu wire bonding and reported that using pre-ultrasound, reduced pad metal splash and increased the ball diameter. Using pre-ultrasound can also change the ball interface shape from concave to flatter shape, which is indicative of uniform stress distribution [18,21].

The present paper extends work on the effect of pre-ultrasound on bond strength and splash. For example, it is not clear yet whether using higher pre-ultrasound always decreases pad metal splash, whether there is a critical value of pre-ultrasound or what is the effect of pre-ultrasound on bond geometry and strength. Answers to each of these questions are attempted.

## 2. Experimental

An automatic ESEC 3100 ball bonder (Besi Esec, Cham, Switzerland), is used for performing thermosonic ball bonding of 25 μm diameter 99.99% Cu wire (MK Electron Co., Ltd., Yongin, Korea). The ultrasound frequency is 128 kHz. The breaking load and elongation of the Cu wire are 10.7 gf and 14.7%, respectively. Bonding is performed at a nominal heater temperature of 150 °C, which results in an actual temperature ≈138 °C at the bonding pad. To

* Corresponding author.
*E-mail address:* arezvani@uwaterloo.ca (A. Rezvani).

0026-2714/$ - see front matter © 2013 Published by Elsevier Ltd.
http://dx.doi.org/10.1016/j.microrel.2013.03.003

ensure adequate statistical reliability, each measurement repeated 10 times (sample size of 10). A commercial ceramic bottleneck capillary having a hole diameter of 35 μm and a chamfer diameter of 51 μm is used. To prevent oxidation of the Cu free air ball during the electronic flame off process, a homogeneous mixture of 95% $N_2$ and 5% $H_2$ is used as a shielding gas. The flow rate of the shielding gas is set to 0.49 l/min. Test chips (Besi Esec, Cham, Switzerland) with bond pads made of 2 μm thick pure Al metalization over a polysilicon layer, were used for ball bonding process. The chips were attached to PLCC44 Ag leadframes. An optical micrograph of the chip after being bonded is shown in Fig. 1.

### 2.1. Process optimization

Ball bonding processes are optimized using a procedure described in [9]. This procedure includes four steps: (a) wedge bond optimization; (b) free air ball optimization; (c) ball bond impact force optimization; and (d) ball bond ultrasound optimization.

The wedge bonding parameters are shown in Table 1. These parameters result in symmetrical bonds without any signs of fish tailing. In Table 1 "%" is used for the ultrasonic vibration amplitude, where 1% is equivalent to a peak to peak vibration amplitude of 26.6 nm measured at the center of the horn tip.

Next, the electronic flame off parameters are optimized to obtain a 50 μm diameter free air ball. The electronic flame off optimization procedure is similar to that described in [9]. A SEM micrograph of a typical 50 μm free air ball is shown in Fig. 2.

The ultrasound and bond force profiles used for the ball bonding are shown in Fig. 3. In contrast to a conventional impact deformation process where no ultrasound is applied during the impact segment, in this process, a pre-defined value of ultrasound (called pre-ultrasound) is applied during the impact segment. To study the effect of pre-ultrasound on bonding strength and Al pad splash, five ball bonding processes are optimized each corresponding to five levels of pre-ultrasound: 0%, 12.5%, 25%, 37.5% and 50%. The five processes are denoted I, II, III, IV and V, respectively. The value of impact force for each of the five processes is optimized separately to obtain the target bonded ball geometry measured by an optical microscope: bonded ball diameter measured at capillary imprint (BDC) of ≈57 μm and bonded ball height of ≈17 μm. These target values of BDC and ball height are selected so they meet the requirements for bonding on a 70 μm diameter bond pad with 120 μm bond pad pitch. To this end, sample ball bonds are made for different values of impact force ranging between 700 and 1000 mN for each of the five processes. The bond force and ultrasound values are kept constant at 400 mN and 45%, respectively. The bonding time is fixed at 25 ms. The selected ultrasound level is the minimum required ultrasound for ball adhesion for the given bond force, and is taken from [1]. Thus, there is no additional ultrasound effect on the bonded ball geometry. The optimized impact force values for each pre-ultrasound level are shown in Table 2. According to Table 2, for a higher pre-ultrasound level, a lower impact force is sufficient to obtain the target bonded ball geometry. This is due to the acoustic softening effect caused by pre-ultrasound [21].

Next, the bonding ultrasound is optimized for each of the five processes. To this end, ball bonds are made by varying the bonding

**Table 1**
Wedge bond parameters.

| Property | Value |
|---|---|
| Impact force (mN) | 650 |
| Bond force (mN) | 350 |
| Ultrasound (%) | 50 |
| Bond time (ms) | 35 |
| Pre-ultrasound at impact (%) | 30 |

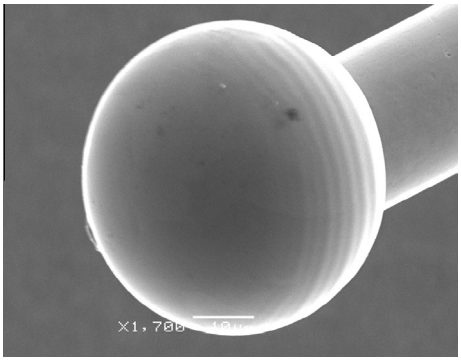

**Fig. 2.** SEM micrograph of a typical 50 μm diameter Cu free air ball.

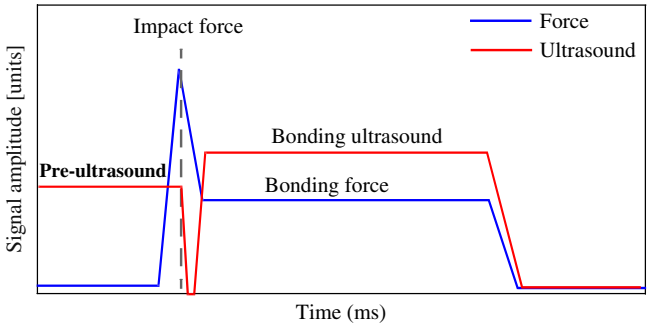


**Fig. 3.** Illustration of the bonding profile of the pre-ultrasound process.

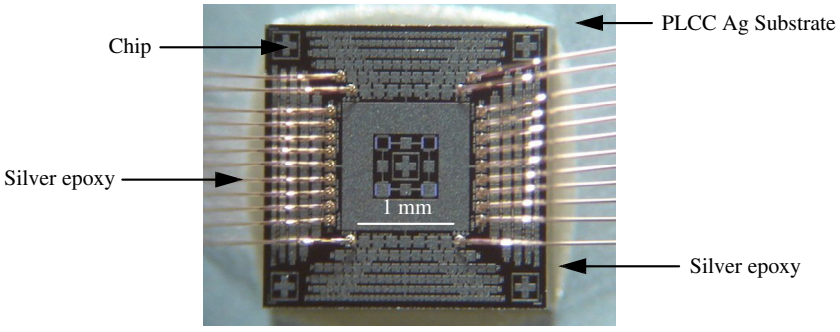


**Fig. 1.** Optical micrograph of the chip used for ball bonding optimization.

**Table 2**
Ball bonding parameter for different samples. impact force is the optimized impact force for each pre-ultrasound level, and bond force is bonding force.

| Processes | I | II | III | IV | V |
|---|---|---|---|---|---|
| Pre-ultrasound (%) | 0 | 12.5 | 25 | 37.5 | 50 |
| Impact force (mN) | 1000 | 925 | 900 | 800 | 700 |
| Bond force (mN) | 400 | 400 | 400 | 400 | 400 |

ultrasound from the minimum level required to avoid ball nonstick on pad (NSOP), in steps to high levels which result in heavily deformed bonded balls. A set of twelve bonds bonded with different ultrasound levels is made for each of the five processes. For each measurement, 10 ball bonds are made and their responses are averaged. shown in Table 2.

An optical and SEM micrograph of a typical ball bond are shown in Fig. 4a and b, respectively. The BDC values are measured at the capillary imprint using an optical microscope. Each BDC measurement is the average of the bonded ball diameters in *x*- and *y*-directions at the capillary imprint as shown in Fig. 4a. Then, the bonds are sheared using a standard shear tester and the shear force is measured. The shear height is 4 μm, and the shear direction is opposite to the ultrasound direction. The shear strength of the ball bond is calculated as (shear force)/area, where area = $\pi(BDC/2)^2$ is

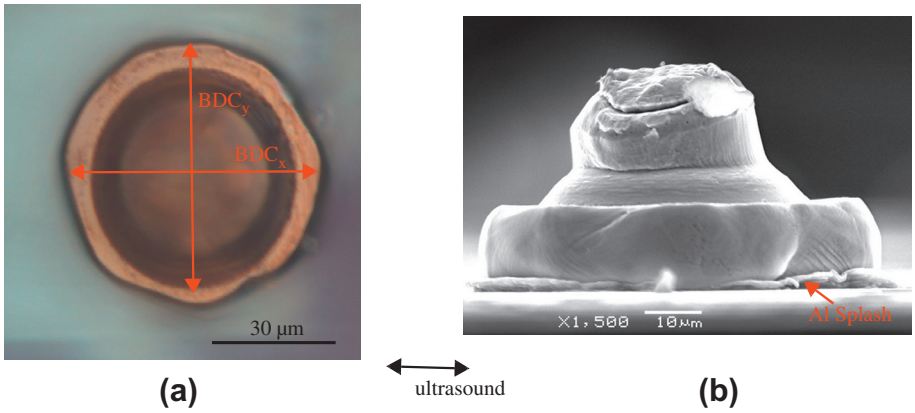


**Fig. 4.** Typical micrograph of bonded ball (a) optical (b) SEM (with wire loop removed for clarity).

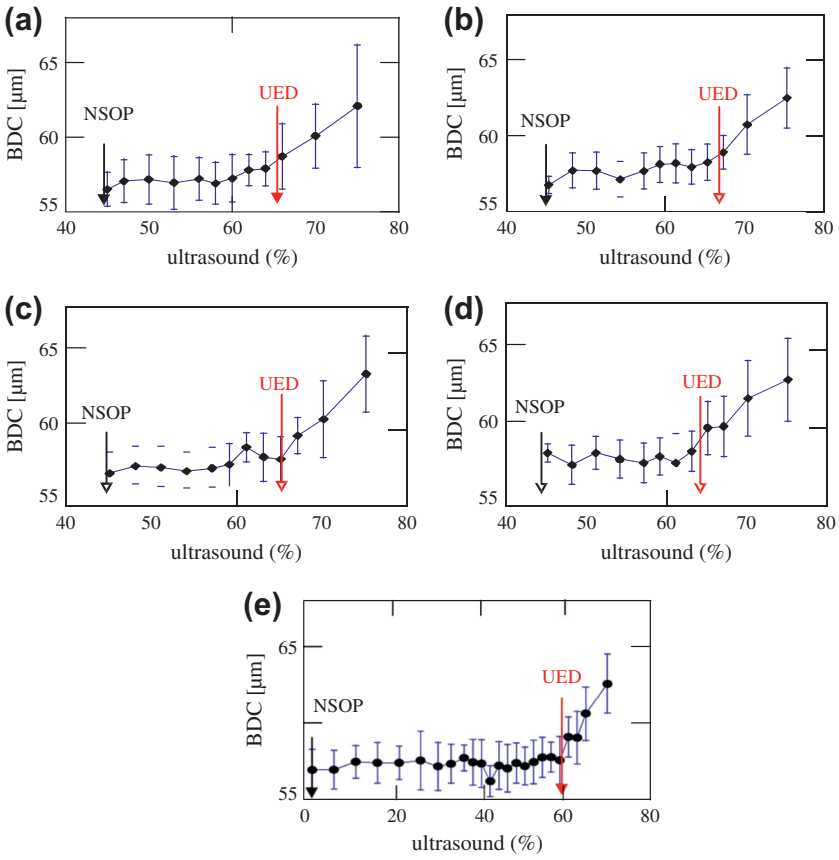


**Fig. 5.** BDC vs. ultrasound for different levels of pre-ultrasound: (a) 0%, (b) 12.5%, (c) 25%, (d) 37.5%, and (e) 50%.

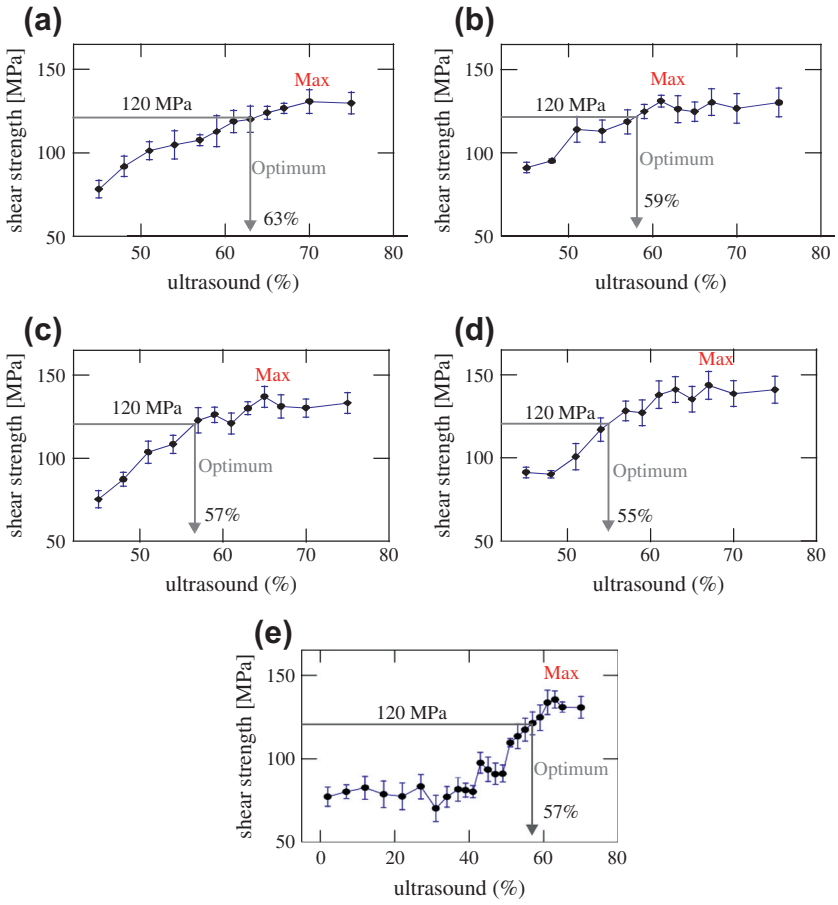


**Fig. 6.** Shear strength vs. ultrasound for different levels of pre-ultrasound: (a) 0%, (b) 12.5%, (c) 25%, (d) 37.5%.

the ball bond cross-sectional area measured at the capillary imprint. The variation in BDC and shear strength with ultrasound are plotted in Figs. 5 and 6 for each of the five processes, respectively. The UED level is selected when a sharp increase in BDC is observed. This is the maximum ultrasound value, at which there is no UED, i.e., the ball deformation is caused primarily due to the normal impact force alone.

### 2.2. Process evaluation

Below a certain ultrasound level, NSOP is observed. This is because a minimum ultrasound level is required for friction, which is the pre-requisite for bonding. According to Fig. 5a–e, the minimum ultrasound needed for bonding is 45% for pre-ultrasound levels 0–37.5% (processes I–IV), and drops to just 2% for pre-ultrasound level of 50% (process V). In the case of process V (pre-ultrasound of 50%), the pre-ultrasound level is higher than the NSOP level (45%). Thus, in the case of process V, the pre-ultrasound contributes to bond growth in contrast to improving deformability alone. The ultrasound level beyond which UED occurs for each of the five processes is shown by the point UED in Fig. 5a–e. With increasing pre-ultrasound level, the UED value decreases gradually (Table 3). This might be attributed to the acoustic softening effect [20,21], which increases the deformability of the bonded ball.

The ball bond shear strength is shown in Fig. 6a–e for each of the five pre-ultrasound processes. The maximum shear strength is shown by the point M for each pre-ultrasound level, and shown in Table 3. It is observed that with increasing level of pre-ultrasound, the bond shear strength also increases. While this is true for pre-ultrasound processes I–IV, however, for process V, the shear strength follows a different trend as shown in Fig. 6e. It is observed that for bonds made with ultrasound levels lower than 43%, the shear strength is relatively constant (80 MPa). This indicates that while the pre-ultrasound level of 50% starts the interfacial bond (microweld) formation, however, the bonding is not completed by pre-ultrasound alone. This is because the pre-ultrasound is active for a very short duration, relative to the bonding ultrasound. Beyond the ultrasound level of 43%, bonding spreads across the interfacial area, resulting in increased shear strength values. Note that the level of 43% is similar to the NSOP of processes I–IV.

In all processes I–V, the maximum shear strength is observed at relatively high ultrasound levels. This is not the desired situation,

**Table 3**
Process responses for samples bonded with different pre-ultrasound levels.

| Process responses | I | II | III | IV | V |
|---|---|---|---|---|---|
| Ultrasound level for UED to happen (%) | 67 | 67 | 66 | 64 | 60 |
| Maximum shear strength (MPa) | 130 | 131 | 136 | 143 | 135 |
| Ultrasound level which result in optimum (120 MPa) shear strength (%) | 63 | 59 | 57 | 55 | 57 |

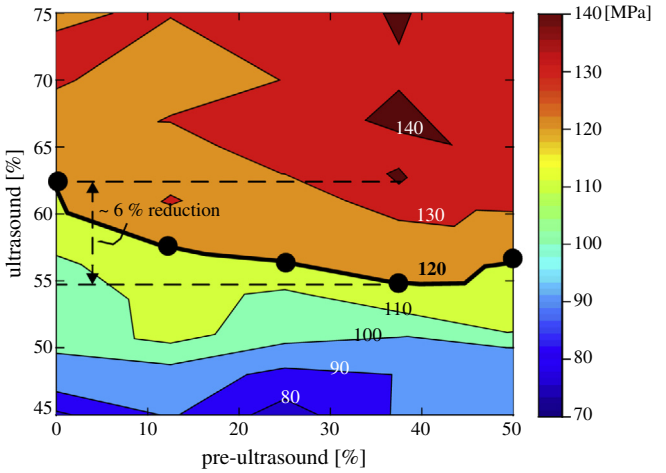


**Fig. 7.** Contour plots of shear strength as a function of ultrasound and pre-ultrasound. As a lower limit for quality shear strength =120 MPa is chosen.

because from [9], it is known that at high ultrasound levels, higher stress is transferred to the pad during bonding. To avoid this, another criterion for comparing the processes can be used. The typical shear strength achieved for Au ball bonding is ≈120 MPa [9]. This can be used as a criterion for comparing the effect of different pre-ultrasound levels. The ultrasound value at which the shear strength of 120 MPa is achieved is denoted by optimum point in Fig. 6a–e and is shown in Table 3. To obtain a minimum shear strength of 120 MPa, the bonding ultrasound values are 63%, 59%, 57%, 55% and 57% for the five pre-ultrasound processes I–V, respectively. The contour plot of the shear strength as a function of pre-ultrasound and ultrasound is shown in Fig. 7. It is observed that for a pre-ultrasound level up to 37.5%, the bonding ultrasound required to obtain a minimum shear strength of 120 MPa decreases with increasing pre-ultrasound level. However, this trend is reversed at pre-ultrasound =50%. This trend is similar to that of maximum shear strength. Up to pre-ultrasound =37.5%, pre-ultrasound provides a surface cleaning, i.e. the higher the pre-ultrasound level, the better the cleaning. However, it does not form welded areas (as NSOP does not change). The reversed trend at pre-ultrasound =50% is probably due to the fact that at this level, there are pre-welded areas bonded during pre-ultrasound application (as NSOP drops to 2%). So, extra ultrasonic energy is not only help bond formation, but destroying some of those pre-welded areas simultaneously.

### 2.3. Splash

Typical SEM and optical micrographs of the sheared surface of a Cu ball bond on Al bond pad are shown in Fig. 8a and b, respectively. In general, when ball bonding with Cu on Al pads, the Al pad metal extrudes out at the periphery of the bonded area. This splash is caused by the higher hardness of Cu ball compared to the Al bond pad material, which contributes to increased wear of the softer material (Al, in this case). On the sheared surface, different characteristic areas are observed. At the outer region, the extruded Al splash is visible by a light gray color, as shown in Fig. 8b. The diameter of this region is named splash diameter. Moving towards the center of the bonded region, a dark ring is observed. This dark ring constitutes the part of splash trapped underneath the ball bulge during bonding. The steep rise in the height of the splash under the ball bulge contributes to its dark appearance under an optical microscope without side light being reflected from this slope into the lens. The diameter of the central bonded region is defined as the ball diameter at interface (BDI). Then the amount of Al pad splash is, splash = splash diameter – BDI.

The variation of splash diameter, BDI and splash with ultrasound for each of the five processes is shown in Fig. 9a–e, respectively. The optimized ultrasound level (ultrasound needed to obtain a shear strength of at least 120 MPa) for each of the five processes is shown by the arrows in Fig. 9a–e, respectively. According to Fig. 9a–d, for pre-ultrasound levels between 0% and 37.5%, an increase in ultrasound value leads to an increase in the splash value. However, at pre-ultrasound = 50%, the value of splash is relatively constant with increasing ultrasound levels for ultrasound levels up to 40%, after which any additional increase in the ultrasound leads to an increase in the splash value. According to Fig. 9, splash diameter is similar for all different pre- ultrasound levels at their optimum point (69–70 μm). The difference in the splash value, comes mainly from their difference in BDI. Up to 37.5%, BDI constantly increases from 45 μm to 51 μm, and splash decreases. The root cause of the increase in BDI, is the application of pre-ultrasound that results in a better cleaning and more uniform distribution of ultrasonic energy, without forming pre-welded areas at the interface. This increases the bonding/adhesion at the interface that results in a larger BDI (extends the bonded area to the more periphery). However, at pre-ultrasound of 50%, the BDI drops to 43 μm, and make the splash larger. This could be due to previously welded areas during pre-ultrasound application. The welded areas might have acted as pinning areas that reduced the effective ultrasonic vibration amplitude (range).

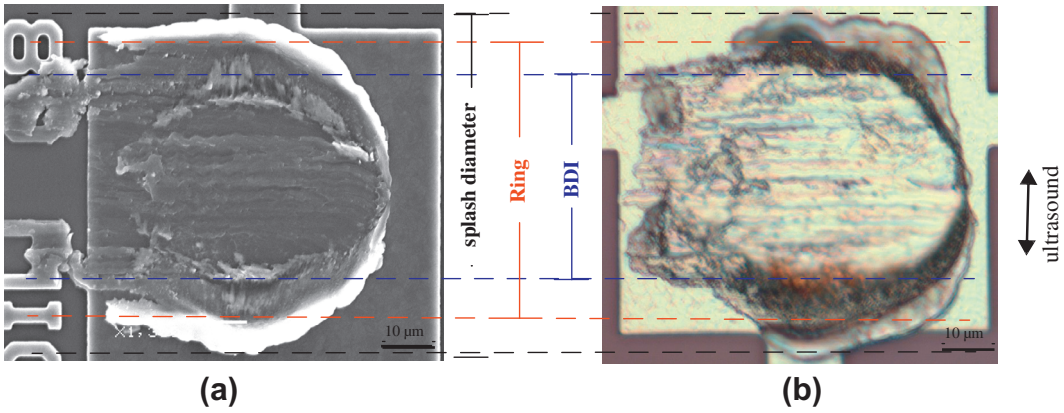


**Fig. 8.** Micrograph of sheared surface of sample bonded with no pre-ultrasound (a) SEM (b) optical.

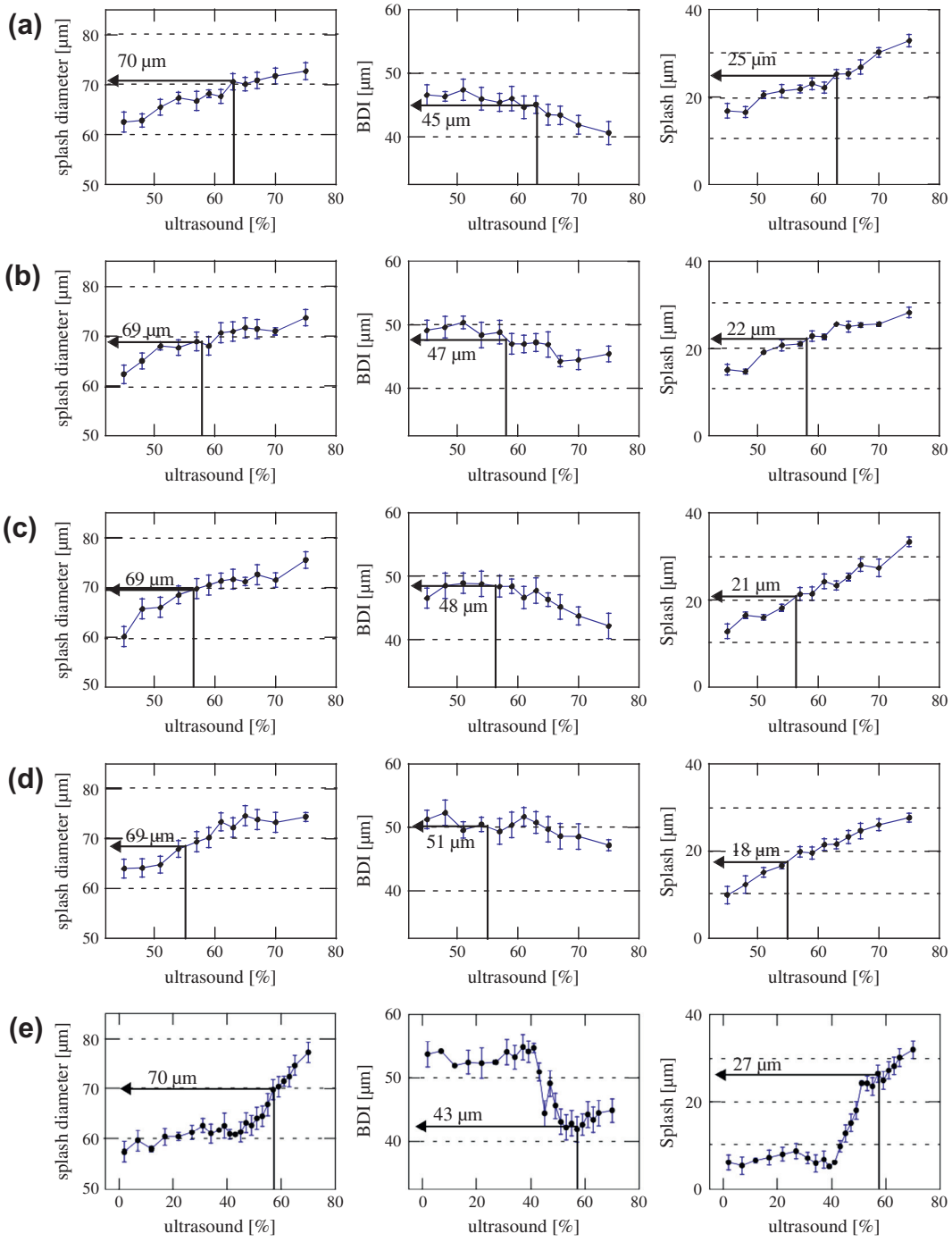


**Fig. 9.** Splash diameter, BDI and Splash vs. ultrasound for different levels of pre-ultrasound: (a) 0%, (b) 12.5%, (c) 25%, (d) 37.5%, and (e) 50%.

**Table 4**
Splash diameter, BDI and splash values at optimum point (120 MPa shear strength) for different pre-ultrasound processes.

| Processes | I | II | III | IV | V |
|---|---|---|---|---|---|
| 120 MPa Shear strength (%) | 63 | 59 | 57 | 55 | 57 |
| Splash diameter (μm) | 70.3 | 69.4 | 69.7 | 68.5 | 69.6 |
| BDI (μm) | 44.9 | 47.5 | 48.4 | 50.7 | 42.9 |
| Splash (μm) | 25.4 | 21.9 | 21.3 | 17.8 | 26.7 |

The values of splash diameter, BDI and splash for optimized bonding ultrasound at each pre-ultrasound level are shown in Table 4. The contour plot of splash as a function of ultrasound and pre-ultrasound is shown in Fig. 10. It is observed that the minimum value of splash is obtained at pre-ultrasound = 37.5%. By using pre-ultrasound = 37.5%, the value of splash can be reduced by ≈7.8 μm, compared to pre-ultrasound = 0%.

## 3. Conclusions

Using super-imposed ultrasound during impact segment (pre-ultrasound) of an impact deformation ball bonding process helps to achieve adequate shear strength at a lower process ultrasound level. It also reduces Al pad splash. It is shown that by adjusting pre-ultrasound to reduce splash also increases the ball/pad inter-

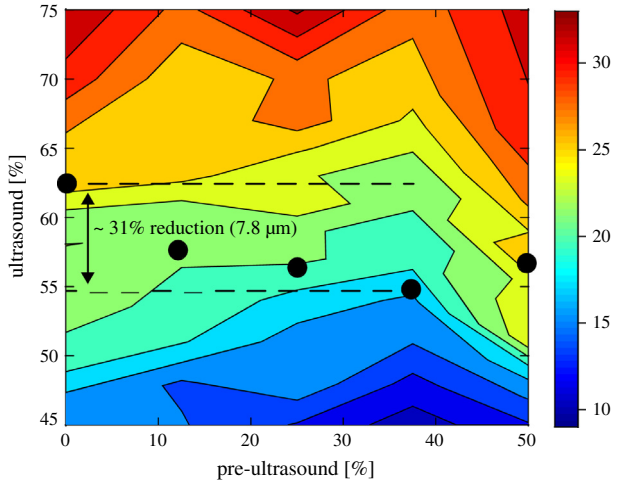


**Fig. 10.** Contour plots of splash as a function of pre-ultrasound and ultrasound. The black circles show the optimized ultrasound parameter (120 MPa shear strength) for each pre-ultrasound level.

face diameter. The reduction of Al pad splash increases the amount of remaining Al, so there is more Al to be corroded/consumed in long-term. This can be helpful for improving long-term reliability.

## Acknowledgments

The authors are grateful for the support of the Natural Science and Engineering Research Council NSERC of Canada, and the Initiative for Automotive Manufacturing Innovation IAMI of Canada.

## References

[1] Shah A, Rezvani A, Mayer M, Zhou Y, Persic J, Moon JT. Reduction of ultrasonic pad stress and aluminum splash in copper ball bonding. Microelectron Reliab 2011;51(1):67–74.
[2] Xu Hui, Liu Changqing, Silberschmidt Vadim V, Chen Zhong, Wei Jun. Initial bond formation in thermosonic gold ball bonding on aluminium metallization pads. J Mater Proces Technol 2010;210(8):1035–42.
[3] Xu H, Liu C, Silberschmidt VV, Chen Z, Wei J, Sivakumar M. Effect of bonding duration and substrate temperature in copper ball bonding on aluminium pads: a TEM study of interfacial evolution. Microelectron Reliab 2011;51(1):113–8.
[4] Rezvani A, Mayer M, Shah A, Zhou N, Hong SJ, Moon T. Free-air ball formation and deformability with Pd coated Cu wire. In: Electronic components and technology conference (ECTC). IEEE; 2011. p. 1516–22.
[5] Nguyen Luu T, McDonald David, Danker Anselm R, Ng Peter. Optimization of copper wire bonding on Al–Cu metallization. IEEE Trans Comp Pack Manuf Tech Part A 1995;18(2):423–9.
[6] Kaimori Shingo, Nonaka Tsuyoshi, Mizoguchi Akira. The development of Cu bonding wire with oxidation-resistant metal coating. IEEE Trans Adv Pack 2006;29(2):227–31.
[7] Srikanth N, Murali S, Wong YM, Vath Charles J. Critical study of thermosonic copper ball bonding. Thin Solid Films 2004;462:339–45.
[8] Deley, Michael, Levine, Lee. The emergence of high volume copper ball bonding. In: Electronics manufacturing technology symposium, 2004. IEEE/CPMT/SEMI 29th International. IEEE; 2004. p. 186–90
[9] Aashish Shah, Mayer Michael, Norman Zhou Y, Hong SJ, Moon JT. Low-stress thermosonic copper ball bonding. IEEE Trans Electron Pack Manuf 2009;32(3):176–84.
[10] Tan Cher Ming, Er Eddie, Hua Younan, Chai Vincent. Failure analysis of bond pad metal peeling using FIB and AFM. IEEE Trans Comp Pack Manuf Technol Part A 1998;21(4):585–91.
[11] Tan Cher Ming, Linggajaya Kaufik, Er Eddie, Chai VS-H. Effect of BOE etching time on wire bonding quality. IEEE Trans Comp Pack Technol 1999;22(4):551–7.
[12] Tan CW, Daud AR. Bond pad cratering study by reliability tests. J Mater Sci: Mater Electron 2002;13(5):309–14.
[13] Caers, J. F. J. M., A. Bischoff, J. Falk, and J. Roggen. "Conditions for reliable ball-wedge copper wire bonding". In Electronic Manufacturing Technology Symposium, 1993, Proceedings of 1993 Japan International, pp. 312–315. IEEE, 1993.
[14] Ho Hong Meng, Tan Yee Chen, Tan Wee Chong, Goh Heng Mui, Toh Boon Hoe, Tan Jonathan. Investigation of factors affecting bonded ball hardness on copper wire bonding. Equip Electron Prod Manuf 2009;11:007.
[15] Wulff, Frank W., C. D. Breach, D. Stephan, and K. J. Dittmer. "Characterisation of intermetallic growth in copper and gold ball bonds on aluminium metallization". In Electronics Packaging Technology Conference, 2004. EPTC 2004. Proceedings of 6th, pp. 348–353. IEEE, 2004.
[16] Wulff, Frank W., C. D. Breach, Dominik Stephan, K. Dittmer Saraswati, and M. Garnier. "Further characterization of intermetallic growth in copper and gold ball bonds on aluminum metallization". Proc. SEMICON Singapore (2005): 35–43.
[17] Hang CJ, Wang CQ, Mayer M, Tian YH, Zhou Y, Wang HH. Growth behavior of Cu/Al intermetallic compounds and cracks in copper ball bonds during isothermal aging. Microelectron Reliab 2008;48(3):416–24.
[18] Rooney Daniel T, Nager Dee Pak, Geiger David, Shanguan Dongkai. Evaluation of wire bonding performance, process conditions, and metallurgical integrity of chip on board wire bonds. Microelectron Reliab 2005;45(2):379–90.
[19] Shah A, Mayer M, Zhou Y, Hong SJ, Moon JT. In situ ultrasonic force signals during low-temperature thermosonic copper wire bonding. Microelectron Eng 2008;85(9):1851–7.
[20] Huang H, Pequegnat A, Chang BH, Mayer M, Du D, Zhou Y. Influence of superimposed ultrasound on deformability of Cu. J Appl Phys 2009;106(11):113514.
[21] Qin I, Shah A, Huynh C, Meyer M, Mayer M, Zhou Y. Role of process parameters on bondability and pad damage indicators in copper ball bonding. Microelectron Reliab 2011;51(1):60–6.